Solid Earth Discuss., 6, 2675–2697, 2014
www.solid-earth-discuss.net/6/2675/2014/
doi:10.5194/sed-6-2675-2014

Solid Earth
Discussions
Open Access

Effective buoyancy ratio: a new parameter to characterize thermo-chemical mixing in the Earth's mantle

A. Galsa, M. Herein, L. Lenkey, M. P. Farkas, and G. Taller

Department of Geophysics and Space Sciences, Eötvös Loránd University, Budapest, Hungary

Received: 28 July 2014 – Accepted: 1 August 2014 – Published: 1 September 2014

Correspondence to: A. Galsa (gali@pangea.elte.hu)

Published by Copernicus Publications on behalf of the European Geosciences Union.

Abstract

Numerical modeling has been carried out in a 2-D cylindrical shell domain to quantify the evolution of a primordial dense layer around the core mantle boundary. Effective buoyancy ratio, B_{eff} was introduced to characterize the evolution of the two-layer thermo-chemical convection in the Earth's mantle. B_{eff} decreases with time due to (1) warming the compositionally dense layer, (2) cooling the overlying mantle, (3) eroding the dense layer by thermal convection in the overlying mantle, and (4) diluting the dense layer by inner convection. When B_{eff} reaches the instability point, $B_{\text{eff}} = 1$, effective thermo-chemical convection starts, and the mantle will be mixed ($B_{\text{eff}} = 0$) during a short time. A parabolic relation was revealed between the initial density difference of the layers and the mixing time. Morphology of large low shear velocity provinces as well as results from seismic tomography and normal mode data suggest a value of $B_{\text{eff}} \geq 1$ for the mantle.

1 Introduction

The most prominent feature of the lowermost part of the Earth's mantle is the two seismically slow domains beneath Pacific and Africa (e.g. Dziewonski et al., 1993; Garnero et al., 2007a). The nearly antipodal large low shear velocity provinces (LLSVPs) are characterized by −2 to −4 % shear wave and −1 to −2 % pressure wave anomaly, several thousand kilometers lateral extent and 800–1000 km elevation from the core mantle boundary (CMB) (Mégnin and Romanowicz, 2000; Masters et al., 2000; Lay, 2005; Zhao, 2009). The margins of the anomalies, where the lateral shear wave velocity gradients are the most pronounced, have sharp sides (Ni et al., 2002; Wang and Wen, 2004; Ford et al., 2006; Garnero and McNamara, 2008) and correlate with hot spot volcanism (Thorne et al., 2004; Torsvik et al., 2010). The existence and the morphology of LLSVPs cannot be satisfactorily explained by the variation in temperature, mineralogical phases or melts. Compositionally dense and so stable material accumu-

SED
6, 2675–2697, 2014

lated above the CMB is necessary in a consistent mantle model (Trampert et al., 2004; Ishi and Tromp, 2004; Garnero et al., 2007b; Bull et al., 2009).

A compositionally dense layer around the core is expected to hinder the mantle convection by reducing the heat transport from the Earth's core (Nakagawa and Tackley, 2004). Thus a chemically dense layer at the base of the mantle has a stabilizing role (Sleep, 1988; Deschamps and Tackley, 2009). On the other hand, the heat coming from the core is trapped in the dense layer that leads to a hot and unstable bottom thermal boundary layer. The dominant process of the two opposite effects can be predicted by the buoyancy ratio (Davaille et al., 2002),

$$B = \frac{\beta}{\alpha \Delta T_{\mathrm{m}}}, \tag{1}$$

which is the ratio of the stabilizing chemical density difference and the destabilizing thermal density difference. β denotes the relative chemical density difference between the layers, α is the thermal expansion coefficient and ΔT_{m} is the temperature difference across the mantle. When B is larger than one, the dense layer is thought to be stable, but in case of $B < 1$, the density decrease by thermal expansion is strong enough to break up and mix it with the overlying mantle by thermo-chemical convection (TCC).

As early as in the eighties pioneer numerical simulations were made to investigate the effect of the compositionally dense lower layer on the mantle dynamics (Christensen and Yuen, 1984; Hansen and Yuen, 1988). Laboratory experiments and numerical models of mantle convection have shown that a chemically dense primordial layer can survive during the age of the Earth if B is large enough (e.g. Davaille et al., 2002; Jellinek and Manga, 2002; Lin and Van Keken, 2006). Depending on the density contrast and the initial thickness of the dense layer thermo-chemical domes/piles are formed in these models which resemble morphologically to the seismological LLSVPs (Trampert et al., 2004; Bull et al., 2009). Deschamps and Tackley (2008, 2009) investigated systematically the influence of some important parameters (depth-, temperature- and concentration-dependent viscosity, internal heating, chemical density contrast,

SED
6, 2675–2697, 2014

mineralogical phase change at 660 km) on the evolution of the initial dense layer and compared the power spectra of density and thermal anomalies obtained from seismic tomography and numerical models. They mapped the parameter space of the thermo-chemical convection and suggested the essential ingredients for a successful mantle convection model.

In these thermo-chemical models B is time-independent during the simulations. However, the primordial dense layer might change greatly due to the heat from the core and possibly from the decay of enriched radioactive elements, the surface erosion of dense material by convection occurring in the overlying mantle, internal convection within the dense layer and termination of subducted slabs at CMB (Nakagawa and Tackley, 2004; Lay, 2005; McNamara and Zhong, 2005; Lay et al., 2006; Garnero et al., 2007a). In this paper we present the results of numerical model calculations made with different values of B including values larger than one. We studied the evolution of the convection and we suggest the introduction of the time-dependent effective buoyancy ratio which characterizes better the dynamics of the TCC.

2 Model description

Boussinesq approximation of the equation system governing the thermo-chemical convection was applied (Chandrasekhar, 1961; Hansen and Yuen, 1988; Čížková and Matyska, 2004). The dimensional equations expressing the conservation of mass, momentum as well as the heat and the mass transport are

$$\frac{\partial u_i}{\partial x_i} = 0, \tag{2}$$

$$0 = \rho g e_i - \frac{\partial p}{\partial x_i} + \frac{\partial \sigma_{ij}}{\partial x_j}, \tag{3}$$

SED
6, 2675–2697, 2014

$$\frac{\partial T}{\partial t} = \kappa \frac{\partial^2 T}{\partial x_i^2} - u_i \frac{\partial T}{\partial x_i} + Q, \tag{4}$$

$$\frac{\partial c}{\partial t} = -u_i \frac{\partial c}{\partial x_i}, \tag{5}$$

where the unknown variables are the density, the pressure, the flow velocity, the temperature of the fluid and the concentration of the dense material, ρ, p, u_i, T and c, respectively. In a two-dimensional model domain there are five equations to determine six variables. Therefore a simple linear relation is given among the density, the temperature and the concentration by the equation of state,

$$\rho = \rho_R \left[1 - \alpha (T - T_S) + \beta c\right], \tag{6}$$

where ρ_R and T_S denote the reference density and the surface temperature, β is the initial relative density difference between the dense layer and the overlying mantle. Q and σ_{ij} are the internal heat production and the deviatoric stress tensor for incompressible Newtonian fluid, respectively. The space coordinates and the time are denoted by x_i and t, respectively; e_i shows the direction of the gravitational acceleration, downwards. According to the Boussinesq approximation other parameters in Eqs. (2)–(6) are supposed to be constant (Table 1) (Van Keken, 2001). Thus the thermal Rayleigh number characterizing the intensity of the convection is about 6×10^6.

Finite element method was applied to solve the partial differential equation system of Eqs. (2)–(5) using COMSOL Multiphysics software package (Zimmerman, 2006). A field method was applied to calculate the concentration distribution of dense material. Two-dimensional cylindrical shell geometry was used to approximate the shape of the Earth's mantle. Geometrical scaling was adopted from Van Keken (2001) to maintain the ratio of the CMB and Earth surface ($\cong 0.3$) and not to overstate the role of the deep mantle, thus the outer and inner radius of the mantle were 4123 km and 1238 km, respectively. The boundaries were isothermal as well as symmetrical and impermeable with respect to the velocity and the concentration.

SED
6, 2675–2697, 2014

Simulation was started from a quasi-stationary state of the temperature field obtained from a chemically homogeneous, purely thermal convection model. Concentration of dense material was set to 1 for the dense layer and 0 above, the transition was adjusted using a smoothed Heaviside function with continuous first derivative and interval thickness of 50 km. The initial thickness of the dense layer was 300 km around the core. Maximum element size was 50 km within the model domain, 30 km along the surface as well as 15 km along the CMB and the surface of the initial dense layer (300 km above the CMB) to ensure the sharp variation in the thermal and/or chemical boundary layer.

During the systematical model calculations the mantle was taken isoviscous without internal heating. The only parameter modified during the simulation was the initial relative density difference between the dense layer and the light overlying mantle, β, it ranged between 0–8 %. We investigated the effect of β on the monitoring parameters: heat flux, velocity, temperature and concentration time series were calculated in the upper and the lower layer. From here we use the lower and upper layer expression in geometrical meaning as the deepest 300 km thick part of the mantle and the overlying zone, respectively. Indices S, D and CMB denote the values at the surface, the top of the lower layer and the CMB, respectively. Table 2 summarizes the monitoring parameters. In addition, we compiled a model with complex rheology (depth-, temperature and composition-dependent viscosity) and composition-dependent internal heating to test their influence on the variation in the effective buoyancy ratio.

3 Results

Figure 1 illustrates the influence of a basal dense layer on the heat flux, velocity, temperature and concentration time series (left) as well as on the evolution of the concentration and temperature field (right). The initial density difference was $\beta = 6\,\%$ between the layers that results in $B = 1$ for the buoyancy ratio. The initial state (stage a) is given by a temperature field obtained from a purely thermal convection calculation and a compositionally dense basal layer placed instantaneously above the CMB. In approx.

1 Gyr (stage b) two-layer convection is being evolved separately in the upper and the lower layers. Inner convection within the dense layer and cold downwellings in the overlying mantle deform the surface of the dense layer. At this stage the temperature of the dense layer reaches its maximum (T_1), and the heat flux (q_S, q_{CMB}, q_D) decreases to a low quasi-stationary level. The erosion of the dense layer by thermal convection in the overlying mantle reduces the concentration of the dense material in the lower layer (c_1) and increases it in the upper one (c_0). The concentration variation shows a linear trend. A similar linear reduction in the volume of the dense layer was found by Zhong and Hager (2003) who studied the entrainment of the dense material by one stationary thermal plume. 4.5 Gyr later (stage c) the dense layer disintegrates, it becomes unstable and effective thermo-chemical convection (TCC) starts. The TCC mixes the layers quickly, the flow accelerates (v_0, v_1), the heat flux (q_S, q_{CMB}, q_D) increases, the dense layer cools (T_1), while the upper layer warms (T_0). The mass flux of the dense material (q_{DC}) starts up and the heterogeneity of the concentration (c_{het}, normalized standard deviation of the concentration) decreases suddenly. In other words, the thermal energy of the dense layer transforms to kinetic energy during a short time. At 5.1 Gyr (stage d) the dense layer ceased, it has been mixed in the mantle, the system reached the stable state. Time series converge to the values characterizing the pure thermal convection, concentration time series tend to the average value, 0.0538. The heat flux (q_S, q_{CMB}, q_D) and velocity (v_0, v_1) time series have higher values and larger fluctuations than in the two-layer convection regime (from stage a to d) that underlines the retaining role of the chemically dense bottom layer. Of course, the homogenization continues protractedly, and after 7.8 Gyr (stage e) the heterogeneity (c_{het}) decreases below 1 %. The heating of the mantle (T) requires Gyrs.

Figure 1 illustrates that although the buoyancy ratio is $B = 1$ – that is the stabilizing chemical density difference and the destabilizing thermal density difference is balanced –, the dense layer evolves considerably, moreover disappears during about 5 Gyr. Additional model calculations revealed that mixing of the layers occurred for both $B < 1$ ($\beta < 6\,\%$) and $B > 1$ ($\beta > 6\,\%$). Therefore, we suggest introducing the effective buoyancy ratio in order to characterize the evolution of the dense layer and the dynamics of the thermo-chemical convection. The effective buoyancy ratio,

$$B_{\text{eff}}(t) = \frac{\beta\ (c_1(t) - c_0(t))}{\alpha\ (T_1(t) - T_0(t))} = \frac{\beta\ \Delta c(t)}{\alpha\ \Delta T(t)}, \tag{7}$$

is time-dependent and includes Δc concentration and ΔT temperature differences between the bottom layer (i.e. the lower 300 km of the mantle) and the overlying mantle.

Figure 2 shows the concentration and temperature differences between the layers as well as the calculated effective buoyancy ratio at different values of β. As the dense layer warms up by the heat coming from the core and the overlying mantle cools down by the retained heat transport due to two-layer convection, the temperature difference increases. It results in the initial rapid decrease of B_{eff}. The concentration difference is decreased monotonically by the erosion of the dense material that later becomes the dominant process in reduction of B_{eff}. When the effective buoyancy ratio reaches the value of $B_{\text{eff}} = 1$, that is the instability point of the system (stage c in Fig. 1), one-layer thermo-chemical convection (mixing) starts. Mixing results in the quick reduction of the temperature and concentration differences. When the effective buoyancy ratio reaches the value of $B_{\text{eff}} = 0$ (stage d in Fig. 1), the dense layer ceases, the mantle becomes mixed. Overturns of dense material cause temporarily negative values in B_{eff}, especially in cases of lower initial density contrast (β). It is obvious that larger initial density contrast entails more stable layering, however the mixing occurs in each model even for $B > 1$.

We attribute the occurrence of the effective thermo-chemical convection in each model to four main physical processes:

1. Heat coming from the core warms up the dense layer reducing its density by thermal expansion.

2. Overlying mantle cools down by retained heat transport due to two-layer convection.

SED
6, 2675–2697, 2014

A. Galsa et al.

3. Thermal convection forming in the upper layer erodes the surface of the dense layer by viscous drag.

4. Inner convection within the dense layer intermixes light material from the overlying mantle.

Processes (1) and (2) result in the increase of the temperature difference between the layers, the processes (3) and (4) cause the decrease of the concentration difference. While the first two phenomena are constrained by the total temperature drop across the mantle (practically $\Delta T_m/2$, see Fig. 2b), the latter two are not. Erosion (3) and dilution (4) gradually reduce the chemical density difference between the layers until the system reaches the instability point ($B_{eff} = 1$) when mixing begins. Mixing occurs in every case, even if the time might exceed the Earth's age ($B \geq 1$). Figure 3 illustrates the phenomena of the erosion and dilution of the dense layer in the concentration and the temperature fields. Black arrows denote the mass flux of the dense material in Fig. 3a and the velocity of the flow in Fig. 3b.

We investigated how the occurrence time of the two most characteristic events (the onset and the end of the effective TCC) depends on the initial chemical density difference, β (Fig. 4a). Obviously, larger β results in more stable, long-lived dense layer and larger occurrence time. A parabolic relation was found between the occurrence time of $B_{eff} = 1$ (onset of mixing) and β. Davaille (1999) observed a similar relation in her laboratory experiments studying the effect of the buoyancy ratio (and other parameters) on the entrainment rate. Parabolic function fits well on data of $B_{eff} = 0$ (end of mixing) too.

As it was shown in Fig. 2, both the erosion/dilution phase (to stage c) and the effective TCC phase (between stage c and d) can be characterized by a linear decrease in Δc. The effective buoyancy ratio displays a similar feature apart from its initial phase, which is due to the transient heating of the dense layer and the cooling of the overlying mantle (from stage a to b). Figure 4b illustrates the slope of the linear curves fitted on Δc and B_{eff} time series during the erosion/dilution phase. It is established that larger initial density contrast (β or B) entails more stable layering owing to the less effec-

SED
6, 2675–2697, 2014

tive erosion/dilution process. Figure 4b presents a power function relation between the slopes of time series (Δc or B_{eff}) and β. Both the parabolic relation in Fig. 4a and the power function relation in Fig. 4b support the idea that mixing of the layers occurs for arbitrary density contrast. It is worth noting that the effective TCC phase demonstrates also a linear decrease in Δc and B_{eff}, but with steeper slope (Fig. 2). The slope of the linear curves fitted on the time series shows a slight decrease as β increases (not shown).

4 Discussion and conclusions

A new parameter, the effective buoyancy ratio, B_{eff} was defined to characterize the dynamics of thermo-chemical convection occurring in the Earth's mantle. Buoyancy ratio, B, in its classical meaning (Davaille et al., 2002) forecasts the resistivity of the dense layer against mixing, however it is insensitive to its behavior. Additionally, our calculations show that mixing also occurs in case of $B > 1$ suggesting the instability of two-layer convection for arbitrary value of B (Davaille, 1999). On the other hand, B_{eff} illustrates well the evolution of the initial dense layer above the CMB consisting of four phases: (i) transition phase of warming dense layer; (ii) erosion and dilution of the dense layer; (iii) effective thermo-chemical convection (mixing of layers); (iv) homogenization.

These conclusions were drawn from a simple isoviscous model. However, the TCC leading to the dissolution of the dense layer strongly depends on the viscosity. Therefore, a more complex model including depth-, temperature- and composition-dependent viscosity and composition-dependent internal heating was calculated in order to investigate the dynamics of the TCC and the variation of the effective buoyancy ratio. Parameters controlling the viscosity and the internal heating were assigned based on the results of Deschamps and Tackley (2008, 2009). An Arrhenius-type law determined the depth- and temperature-dependence of the viscosity, which increased one order of magnitude from the surface to the CMB and decreased 6 orders of magnitude with the temperature. A viscosity jump with a factor of 30 was superimposed at the depth of 660 km reflecting the effect of mineralogical phase change on the viscosity. The viscosity of the dense material ($c = 1$) is half of that of the light material ($c = 0$) with a linear transition. Internal heating was adjusted to produce 65 mW m^{-2} average heat flux on the surface, but the heat production of the dense material was increased by a factor of 10 due to the higher abundance of radioactive elements. The initial compositional density contrast between the layers was $\beta = 6\,\%$ correspondingly to the model presented in Fig. 1. Simulation started from a quasi-stationary state of the temperature field obtained from a chemically homogeneous, purely thermal convection model with depth- and temperature-dependent viscosity and homogeneous internal heating.

Figure 5 illustrates the pattern of the TCC for the complex model at 3.5 Gyr after the inset of the dense layer when the effective buoyancy ratio is approx. 1.13. During 3.5 Gyr the dense layer disintegrated and two hot, compositionally dense, nearly antipodal piles formed with sharp sides. Due to the concentration-dependent internal heating the temperature within piles exceeds the CMB temperature thus the viscosity decreases considerably. The concentration and velocity field attest that a sluggish internal convection forms within the piles. A stagnant lid regime evolved owing to the strongly temperature-dependent viscosity (Solomatov, 1995) which does not participate in the convection. Beneath the stagnant lid vivid small-scale convection occurs in the upper mantle (Kuslits et al., 2014). Due to the lack of the endothermic phase transition advective mass and heat transport exists between the upper and lower mantle.

Figure 2 displays the variation of the concentration and temperature differences between the layers and the effective buoyancy ratio for the "mantle-like" model (mm_6 %). As a consequence of the stagnant lid regime ΔT decreased compared to the isoviscous case but the character of the curve remained similar. The rate of the decrease in Δc by erosion and dilution processes became steeper owing to the reduced viscosity of the hot, dense thermo-chemical layer. As a result the effective buoyancy ratio has a similar nature with steeper erosion/dilution phase and less steep mixing phase. In summary, the stability of the dense layer in the complex model with varying viscosity and internal heating was reduced compared to isoviscous model by about 20 %, but the physical processes acting in the two models were the same.

In order to make a comparison among different numerical models Tackley (2012) rescaled the results for the heat expansion of $\alpha = 10^{-5}\,1\,\mathrm{K}^{-1}$, as a more realistic value in the deep, compressible mantle (Mosenfelder et al., 2009). Applying smaller heat expansion requires less initial compositional density contrast to obtain the same B_{eff}. Rescaling our model (Fig. 1) for reduced heat expansion minimum $\beta = 3\,\%$ initial compositional density contrast is needed to maintain the dense layer over the age of the Earth. It is in accordance with the results of Tackley (2012) who arrived to density difference of 2–3 % based on different model calculations.

Trampert et al. (2004) using tomographic likelihoods separated the total density variation in the mantle into temperature and chemical density variation. They established that the present compositional density variation is dominant in the lower 1000 km of mantle and it is likely to exceed 2 %. It corresponds to our models with initial density contrast of $\beta = 3\,\%$ assuming reduced heat expansion, because the density difference decreases gradually due to erosion and dilution processes (Fig. 2).

Several normal modes of the Earth show a significant sensitivity to the density/shear velocity ratio in the deep mantle (Koelemeijer et al., 2012). Ishi and Tromp (2004) revealed a total density increment of approx. 0.5 % beneath Africa and Pacific in which the opposite effect of the temperature and the compositional variation is superimposed. Taking into account that the compositional density increase of more than 2 % and the total density increase of only 0.5 % a rough estimate of the effective buoyancy ratio gives a value of slightly above 1. Based on our model results at this stage the TCC system in the Earth's mantle might be just before the instability point. It agrees well with the present strongly deformed, disintegrated morphology of LLSVPs (e.g. Garnero et al., 2007a).

Author contribution. A. Galsa built up and tested the model, A. Galsa, M. P. Farkas and G. Taller ran and evaluated the simulations. A. Galsa, M. Herein and L. Lenkey interpreted the results and A. Galsa prepared the manuscript with the contribution of all authors.

SED
6, 2675–2697, 2014

Acknowledgements. The authors are grateful to Paul J. Tackley for his constructive remarks. This research was supported by the European Union and the State of Hungary, co-financed by the European Social Fund in the framework of TÁMOP 4.2.4. A/1-11-1-2012-0001 "National Excellence Program". This research was also supported by the Hungarian Scientific Research Fund (OTKA K-72665 and OTKA NK100296) and it was implemented thanks to the scholarship in the framework of the TÁMOP 4.2.4.A-1 priority project.

References

Bull, A. L., McNamara, A. K., and Ritsema, J.: Synthetic tomography of plume clusters and thermochemical piles, Earth Planet. Sc. Lett., 278, 152–162, 2009.

Chandrasekhar, S.: Hydrodynamic and Hydromagnetic Stability, Clarendon, Oxford, 1961.

Christensen, U. R. and Yuen, D. A.: The interaction of a subducting lithospheric slab with a chemical or phase boundary, J. Geophys. Res., 89, 4389–4402, 1984.

Čížková, H. and Matyska, C.: Layered convection with an interface at a depth of 1000 km: stability and generation of slab-like downwellings, Phys. Earth Planet. In., 141, 269–279, 2004.

Davaille, A.: Two-layer thermal convection in miscible viscous fluids, J. Fluid Mech., 379, 223–253, 1999.

Davaille, A., Girard, F., and Le Bars, M.: How to anchor hotspots in a convecting mantle?, Earth Planet. Sc. Lett., 203, 621–634, 2002.

Deschamps, F. and Tackley, P. J.: Searching for models of thermo-chemical convection that explain probabilistic tomography I – principles and influence of rheological parameters, Phys. Earth Planet. In., 171, 357–373, 2008.

Deschamps, F. and Tackley, P. J.: Searching for models of thermo-chemical convection that explain probabilistic tomography II – influence of physical and compositional parameters, Phys. Earth Planet. In., 176, 1–18, 2009.

Dziewonski, A. M., Foret, A. M., Su, W.-J., and Woodward, R. L.: Seismic tomography and geodynamics, in: Relating Geophysical Structures and Processes, The Jeffreys Volume, AGU Geophysical Monograph, 76, Washington, DC, 67–105, 1993.

Ford, S. R., Garnero, E. J., and McNamara, A. K.: A strong lateral shear velocity gradient and anisotropy heterogeneity in the lowermost mantle beneath the southern Pacific, J. Geophys. Res., 111, B03306, doi:10.1029/2004JB003574, 2006.

SED
6, 2675–2697, 2014

Effective buoyancy ratio

A. Galsa et al.

Garnero, E. J. and McNamara, A. K.: Structure and dynamics of Earth's lower mantle, Science, 320, 626–628, 2008.
Garnero, E. J., Thorne, M. S., McNamara, A. K., and Rost, S.: Fine-scale ultra-low velocity zone layering at the core-mantle boundary and superplumes, in: Superplumes, Springer, 139–158, 2007a.
Garnero, E. J., Lay, T., and McNamara, A. K.: Implications of lower-mantle structural heterogeneity for existence and nature of whole-mantle plumes, in Plates, plumes, and planetary processes, Geol. Soc. Am. Special Paper, 79–101, doi:10.1130/2007.2430(05), 2007b.
Hansen, U. and Yuen, D. A.: Numerical simulations of thermal-chemical instabilities at the core–mantle boundary, Nature, 334, 237–240, 1988.
Ishii, M. and Tromp, J.: Constraining large-scale mantle heterogeneity using mantle and inner-core sensitive normal modes, Phys. Earth Planet. In., 146, 113–124, 2004.
Jellinek, A. M. and Manga, M.: The influence of a chemical boundary layer on the fixity, spacing and lifetime of mantle plumes, Nature, 418, 760–763, 2002.
Koelemeijer, P. J., Deuss, A., and Trampert, J.: Normal mode sensitivity to Earth's D″ layer and topography on the core-mantle boundary: what we can and cannot see, Geophys. J. Int., 190, 553–568, 2012.
Kuslits, L. B., Farkas, M. P., and Galsa, A.: Effect of temperature-dependent viscosity on mantle convection, Acta Geod. Geophys., 49, 249–263, doi:10.1007/s40328-014-0055-7, 2014.
Lay, T.: The deep mantle thermo-chemical boundary layer: The putative mantle plume source, in: Plates, Plumes, and Paradigms, Geol. Soc. Am. Bull., 338, 193–205, 2005.
Lay, T., Hernlund, J., Garnero, E. J., and Thorne, M. S.: A post-perovskite lens and D″ heat flux beneath the Central Pacific, Science, 314, 1272–1276, 2006.
Lin, S.-C. and Van Keken, P. E.: Dynamics of thermochemical plumes: 1. Plume formation and entrainment of a dense layer, Geochem. Geodyn. Geosyst., 7, Q02006, doi:10.1029/2005GC001071, 2006.
Masters, G., Laske, G., Bolton, H., and Dziewonski, A. M.: The relative behavior of shear velocity, bulk sound speed, and compressional velocity in the mantle: implications for chemical and thermal structure in Earth's deep interior, in: Mineral Physics and Tomography From the Atomic to the Global Scale, AGU, Washington, DC, 63–87, 2000.
McNamara, A. K. and Zhong, S.: Thermochemical structures beneath Africa and the Pacific Ocean, Nature, 437, 1136–1139, 2005.

SED
6, 2675–2697, 2014

Mégnin, C. and Romanowicz, B.: The three-dimensional shear-velocity structure of the mantle from the inversion of body, surface and higher-mode waveforms, Geophys. J. Int., 143, 709–728, 2000.

Mosenfelder, J. L., Asimow, P. D., Frost, D. J., Rubie, D. C., and Ahrens, T. J.: The $MgSiO_3$ system at high pressure: thermodynamic properties perovskite, postperovskite, and melt from global inversion of shock and static compression data, J. Geophys. Res., 114, B01203, doi:10.1029/2008JB005900, 2009.

Nakagawa, T. and Tackley, P. J.: Effect of thermo-chemical mantle convection on the thermal evolution of the Earth's core, Earth Planet. Sc. Lett., 220, 107–119, 2004.

Ni, S., Tan, E., Gurnis, M., and Helmberger, D. V.: Sharp sides to the African superplume, Science, 296, 1850–1852, 2002.

Sleep, N. H.: Gradual entrainment of a chemical layer at the base of the mantle by overlying convection, Geophys. J., 95, 437–447, 1988.

Solomatov, V. S.: Scaling of temperature- and stress-dependent viscosity convection, Phys. Fluids, 7, 266–274, 1995.

Tackley, P. J.: Dynamics and evolution of the deep mantle resulting from thermal, chemical, phase and melting effects, Earth-Sci. Rev., 110, 1–25, 2012.

Thorne, M. S., Garnero, E. J., and Grand, S. P.: Geographic correlation between hot spots and deep mantle lateral shear-wave velocity gradients, Phys. Earth Planet. In., 146, 47–63, 2004.

Torsvik, T. H., Burke, K., Steinberger, B., Webb, S. J., and Ashwal, L. D.: Diamonds sampled by plumes from the core-mantle boundary, Nature, 466, 352–355, 2010.

Trampert, J., Deschamps, F., Resovsky, J., and Yuen, D. A.: Probabilistic tomography maps chemical heterogeneities throughout the lower mantle, Science, 306, 853–856, 2004.

Van Keken, P.: Cylindrical scaling for dynamical cooling models of the Earth, Phys. Earth Planet. In., 124, 119–130, 2001.

Wang, Y. and Wen, L.: Mapping the geometry and geographic distribution of a very low velocity province at the base of the Earth's mantle, J. Geophys. Res., 109, B10305, doi:10.1029/2003JB002674, 2004.

Zhao, D.: Multiscale seismic tomography and mantle dynamics, Gondwana Res., 15, 297–323, 2009.

Zhong, S. and Hager, B. H.: Entrainment of a dense layer by thermal plume, Geophys. J. Int., 154, 666–676, 2003.

SED

6, 2675–2697, 2014

Effective buoyancy ratio

A. Galsa et al.

Zimmerman, W. B. J.: Multiphysics Modeling With Finite Element Methods, World Scientific Publishing Company, Singapore, 2006.

SED
6, 2675–2697, 2014

Table 1. Model constants.

Definition	Symbol	Value
Gravitational acceleration	g	$10\,\mathrm{m\,s^{-2}}$
Dynamic viscosity	η	$10^{22}\,\mathrm{Pa\,s}$
Heat diffusivity	κ	$10^{-6}\,\mathrm{m^2\,s^{-1}}$
Thermal expansivity	α	$2 \times 10^{-5}\,1\,\mathrm{K^{-1}}$
Reference density	ρ_R	$4500\,\mathrm{kg\,m^{-3}}$
Temperature drop across the mantle	ΔT_m	3000 K
Thickness of mantle	d	2885 km

SED
6, 2675–2697, 2014

SED
6, 2675–2697, 2014

Table 2. Monitoring parameters.

Symbol	Definition
q_S	Surface heat flow
q_{CMB}	Heat flow at CMB
q_D	Heat flow at the top of the dense layer
v_0	Rms velocity of the upper layer
v_1	Rms velocity of the lower layer
v	Rms velocity of the mantle
T_0	Temperature of the upper layer
T_1	Temperature of the lower layer
T	Temperature of the mantle
c_0	Concentration of the upper layer
c_1	Concentration of the lower layer
c_{het}	Heterogeneity of the concentration
q_{DC}	Concentration flux at the top of the dense layer
Δc	Concentration difference between the lower and upper layer
ΔT	Temperature difference between the lower and upper layer
B_{eff}	Effective buoyancy ratio

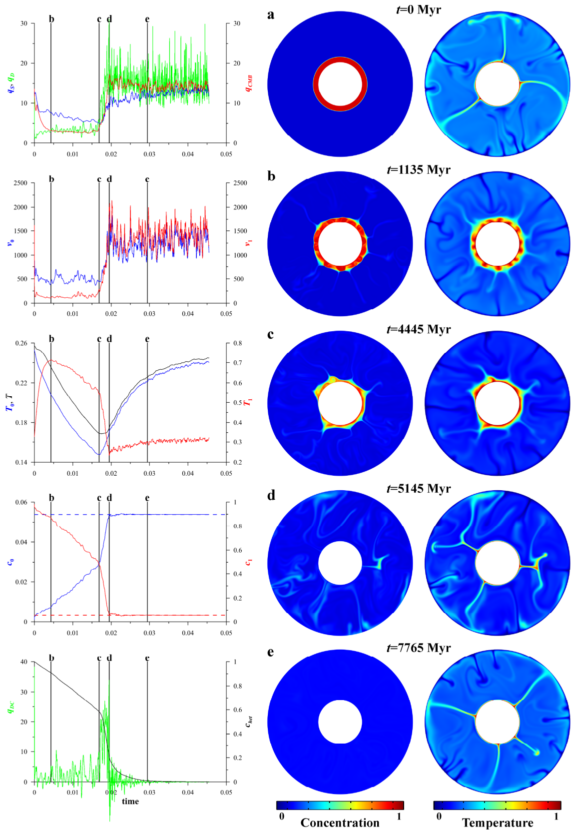

Figure 1. Five stages characterizing the evolution of the thermo-chemical convection. Left: time series of monitoring parameters (heat flux, velocity, temperature, concentration, see in Table 2), vertical lines denote the stages shown in the right side. Right: the evolution of the concentration of the dense material and the temperature field.

SED
6, 2675–2697, 2014
Effective buoyancy ratio
A. Galsa et al.

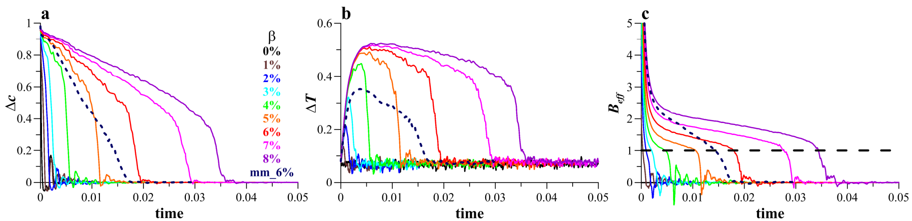

Figure 2. (a) The concentration and **(b)** the temperature differences between the lower and upper layers as well as **(c)** the effective buoyancy ratio as a function of time at different values of the initial compositional density contrast, β. Dashed blue line denotes the complex model (see in text).

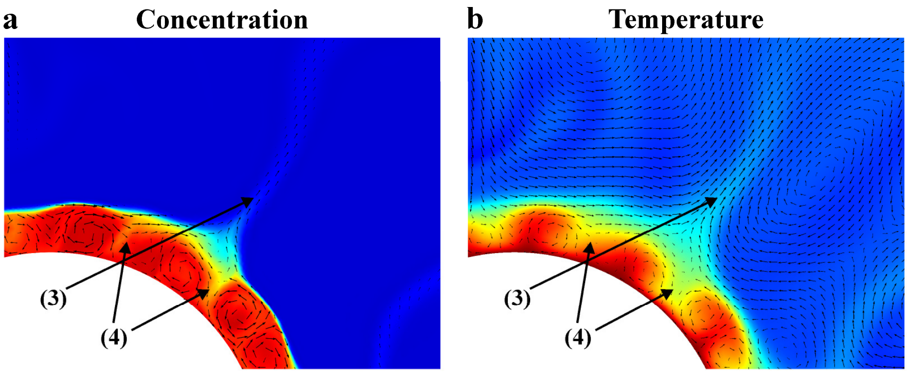

Figure 3. (a) Concentration of the dense material and **(b)** temperature field demonstrating the processes of (3) erosion and (4) dilution of the dense layer. Black arrows denote the logarithmically scaled **(a)** mass flux of the dense material and **(b)** flow velocity.

SED
6, 2675–2697, 2014

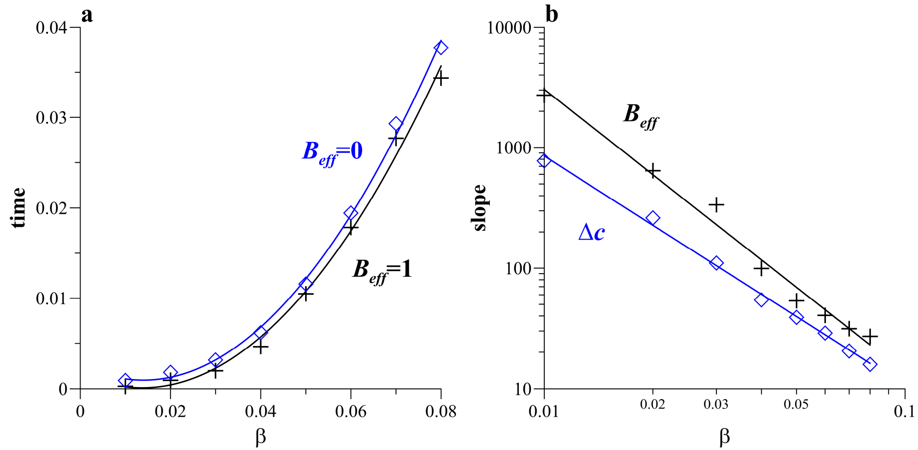

Figure 4. (a) Occurrence time of the two most characteristic events: $B_{\text{eff}} = 1$ (onset of mixing) and $B_{\text{eff}} = 0$ (end of mixing) as well as **(b)** slope of the decrease of the concentration difference and the effective buoyancy ratio during the erosion/dilution phase as a function of β.

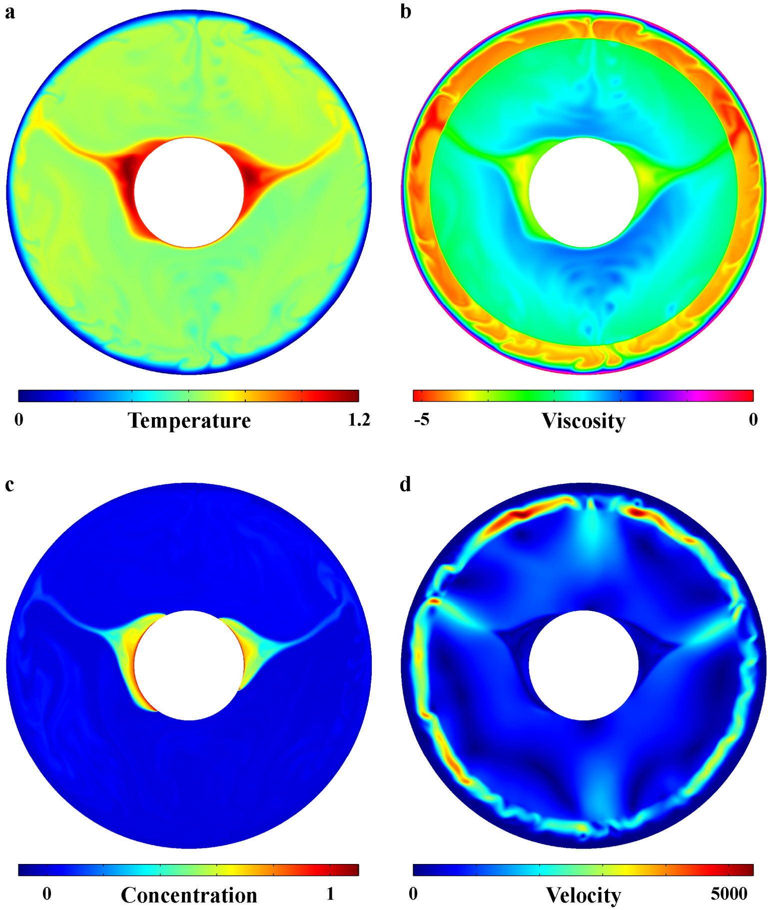

Figure 5. A quasi-stationary state of the **(a)** temperature, **(b)** viscosity, **(c)** concentration of the dense material and **(d)** velocity for the complex model (see text) at 3.5 Gyr (t = 0.01325). Viscosity is scaled logarithmically and non-dimensionalized by divided with the surface viscosity.

SED
6, 2675–2697, 2014

Effective buoyancy ratio

A. Galsa et al.